THE JOURNAL OF BIOLOGICAL CHEMISTRY VOL. 285, NO. 50, pp. 39127–39139, December 10, 2010

Alternatively Expressed Domains of AU-rich Element RNA-binding Protein 1 (AUF1) Regulate RNA-binding Affinity, RNA-induced Protein Oligomerization, and the Local Conformation of Bound RNA Ligands*[S]

Received for publication, August 30, 2010, and in revised form, September 29, 2010 Published, JBC Papers in Press, October 6, 2010, DOI 10.1074/jbc.M110.180182

Beth E. Zucconi[1,2], Jeff D. Ballin[2], Brandy Y. Brewer, Christina R. Ross, Jun Huang, Eric A. Toth, and Gerald M. Wilson[3]

From the Department of Biochemistry and Molecular Biology and Marlene and Stewart Greenebaum Cancer Center, University of Maryland School of Medicine, Baltimore, Maryland 21201

AU-rich element RNA-binding protein 1 (AUF1) binding to AU-rich elements (AREs) in the 3′-untranslated regions of mRNAs encoding many cytokines and other regulatory proteins modulates mRNA stability, thereby influencing protein expression. AUF1-mRNA association is a dynamic paradigm directed by various cellular signals, but many features of its function remain poorly described. There are four isoforms of AUF1 that result from alternative splicing of exons 2 and 7 from a common pre-mRNA. Preliminary evidence suggests that the different isoforms have varied functional characteristics, but no detailed quantitative analysis of the properties of each isoform has been reported despite their differential expression and regulation. Using purified recombinant forms of each AUF1 protein variant, we used chemical cross-linking and gel filtration chromatography to show that each exists as a dimer in solution. We then defined the association mechanisms of each AUF1 isoform for ARE-containing RNA substrates and quantified relevant binding affinities using electrophoretic mobility shift and fluorescence anisotropy assays. Although all AUF1 isoforms generated oligomeric complexes on ARE substrates by sequential dimer association, sequences encoded by exon 2 inhibited RNA-binding affinity. By contrast, the exon 7-encoded domain enhanced RNA-dependent protein oligomerization, even permitting cooperative RNA-binding activity in some contexts. Finally, fluorescence resonance energy transfer-based assays showed that the different AUF1 isoforms remodel bound RNA substrates into divergent structures as a function of protein:RNA stoichiometry. Together, these data describe isoform-specific characteristics among AUF1 ribonucleoprotein complexes, which likely constitute a mechanistic basis for differential functions and regulation among members of this protein family.

In complex organisms, individual cells must precisely control protein expression to rapidly respond to ever-changing stimuli. Protein expression can be regulated at multiple levels, including the rates of transcription, translation, and protein degradation. Messenger RNA stability represents another critical mechanism for regulating protein expression, because alterations in mRNA decay kinetics can modulate the cytoplasmic mRNA concentrations required to program protein synthesis independent of changes in the mRNA synthetic rate. Across the population of cellular mRNAs, decay rates can vary by 2 orders of magnitude or more. Furthermore, the stability of many mRNAs can be dramatically altered in response to selected stimuli (reviewed in Refs. 1, 2).

Information directing the decay kinetics of specific transcripts is located within the mRNAs themselves. The best characterized of these *cis*-acting mRNA stability determinants are the AU-rich elements (AREs)[4] located in the 3′-untranslated regions (3′UTRs) of many labile mRNAs (3). In humans, AREs may be present in as many as 8% of all transcripts, including many that encode clinically significant factors like proto-oncogenes, cytokines, cell cycle regulators, and inflammatory mediators (4). Regulation of mRNA decay through AREs involves the association of cellular *trans*-acting factors, collectively known as ARE-binding proteins (reviewed in Refs. 5, 6); however, more recently, selected microRNAs have been implicated as *trans*-regulators of ARE function (7, 8). Some ARE-binding proteins, like members of the Hu family of proteins, act as stabilizing factors by preventing mRNA decay (9, 10), whereas others, like tristetraprolin (11, 12), KSRP (13, 14), and AUF1 (15–18), are generally associated with enhanced degradation of targeted transcripts. Some other ARE-binding proteins, including TIA-1 and TIAR, do not appear to modulate mRNA decay kinetics directly but rather inhibit their translation (reviewed in Ref. 19).

AUF1, also known as heterogeneous nuclear ribonucleoprotein D (hnRNP D), is a family of four proteins derived from alternative splicing of a common pre-mRNA, named according to their apparent molecular masses as $p37^{AUF1}$,

* This work was supported, in whole or in part, by National Institutes of Health Grant R01 CA102428 from NCI (to G. M. W.).

[S] The on-line version of this article (available at http://www.jbc.org) contains supplemental Fig. 1.

[1] Supported in part by National Institutes of Health Grant T32 GM066706 from NIGMS.

[2] Both authors contributed equally to this work.

[3] To whom correspondence should be addressed: Dept. of Biochemistry and Molecular Biology, University of Maryland School of Medicine, 108 N. Greene St., Baltimore, MD 21201. Tel.: 410-706-8904; Fax: 410-706-8297; E-mail: gwils001@umaryland.edu.

[4] The abbreviations used are: ARE, AU-rich element; Cy3, cyanine-3; DSP, dithio-bis(succinimidyl propionate); Fl, fluorescein; MBDA, macromolecular binding density analysis; RNP, ribonucleoprotein; hnRNP, heterogeneous nuclear ribonucleoprotein; nt, nucleotide.

p40^{AUF1}, p42^{AUF1}, and p45^{AUF1} (20). All isoforms have two tandemly arranged RNA recognition motifs, which are essential for RNA binding, a C-terminal extension that includes a glutamine-rich domain, and an acidic N-terminal region that may contribute to protein dimerization (21, 22). The two largest isoforms also include a 49-amino acid domain near the C terminus encoded by exon 7, whereas p40^{AUF1} and p45^{AUF1} both contain a 19-amino acid insert encoded by exon 2 that is contiguous with RRM1 (Fig. 1*A*). AUF1 was first identified as a cytoplasmic factor that stimulated the decay of c-*myc* mRNA in cell-free mRNA decay assays (23), and it is most frequently associated with acceleration of ARE-directed mRNA decay (described above). However, emerging data indicate that AUF1 may also enhance mRNA translational efficiency in some cases, possibly involving interaction with components of the translation machinery like eIF4G and poly(A)-binding protein (24) or competition for ARE targets between AUF1 and the translational repressor TIAR (25).

Although studies assessing the function of AUF1 in post-transcriptional control of gene expression frequently do not discriminate among the family members, some reports indicate variations in the function and/or regulated expression of individual AUF1 isoforms. First, p42^{AUF1} and p45^{AUF1} are normally nuclear, whereas p37^{AUF1} and p40^{AUF1} are found within both nuclear and cytoplasmic compartments in many cell types (21, 26–28). Second, distinct isoforms have been implicated in the regulated decay of selected ARE-containing mRNAs. For example, a reporter mRNA containing the ARE from interleukin-3 mRNA was stabilized by concomitant siRNA-directed suppression of p40^{AUF1} and p45^{AUF1} but not by coordinated depletion of p42^{AUF1} and p45^{AUF1} or all isoforms simultaneously (17). By contrast, specific overexpression of p37^{AUF1}, and to some extent p40^{AUF1}, destabilized a reporter mRNA containing the ARE from granulocyte-macrophage colony-stimulating factor mRNA, although p42^{AUF1} and p45^{AUF1} had no effect (18). Third, some stimuli have been reported to modulate the cellular levels of specific AUF1 isoforms. In sheep uterus, estradiol increased expression of p45^{AUF1} but not other isoforms (29). Similarly, prostaglandin A_2 specifically increased levels of p45^{AUF1} in H1299 non-small-cell lung carcinoma cells (30). Finally, the differentially expressed sequences that distinguish AUF1 family members provide opportunities for isoform-specific regulation through post-translational events. For example, in THP-1 monocytic leukemia cells, polysome-associated p40^{AUF1} is phosphorylated at two sites encoded by exon 2, which are accordingly absent in p37^{AUF1} and p42^{AUF1} (28). Dephosphorylation of these sites is associated with stabilization of ARE-containing mRNAs coupled with condensation of local RNA structure (28, 31).

Taken together, the potential for differential function and regulation among AUF1 isoforms suggests that each may exhibit unique biochemical characteristics that mediate distinctive RNA-binding paradigms. In this study, we have used biochemical and fluorescence spectroscopic approaches to compare the RNA-binding and RNA structural remodeling properties of all four AUF1 isoforms. Using purified, recombinant AUF1 proteins and two families of model AREs, we show that all AUF1 isoforms assemble into oligomeric protein complexes on ARE substrates through two distinct binding steps. However, the differentially expressed protein domains encoded by exons 2 and 7 each influence the RNA-binding activities of AUF1 proteins in distinct ways, based on variations in RNA-binding affinity, RNA-induced protein oligomerization, and the structural properties of bound RNA substrates. Together, these data are consistent with a model whereby alternative splicing of the AUF1 pre-mRNA generates a family of RNA-binding proteins with diverse biochemical properties, which may contribute to the heterogeneity of AUF1 function and complexity of its regulation.

TABLE 1
RNA substrates used in this study

Name	Sequence (5'→3')
ARE_{44}	CUUGUGAUUAUUUAUUAUUUAUUUAUUAUUUAUUUAUUUACAGA
ARE_{38}	GUGAUUAUUUAUUAUUUAUUUAUUAUUUAUUUAUUUAG
ARE_{35}	GAUUAUUUAUUAUUUAUUUAUUAUUUAUUUAUUUA
ARE_{34}	AUUAUUUAUUAUUUAUUUAUUAUUUAUUUAUUUA
ARE_{30}	UUUAUUAUUUAUUUAUUAUUUAUUUAUUUA
ARE_{24}	AUUUAUUUAUUAUUUAUUUAUUUA
ARE_{20}	UUUAUUAUUUAUUUAUUUAG
ARE_{18}	UUAUUAUUUAUUUAUUUA
fos ARE domain I	UUUUAUUGUUUUAAUUUAUUUAUUAAGAUGGAUUCUCAGAUAUUUA
Rβ	UGGCCAAUGCCCUGGCUCACAAAUACCACUG

EXPERIMENTAL PROCEDURES

RNA Substrates—Synthesis, deprotection of 2′-hydroxyl groups, and purification of all RNA oligonucleotides were performed by Integrated DNA Technologies or Dharmacon. Lyophilized RNA pellets were resuspended in deionized H_2O. RNA yields and fluorophore labeling efficiencies were quantified by absorbance, incorporating fractional contributions of coupled fluorophores to A_{260} for substrates containing fluorescein (Fl) and/or cyanine-3 (Cy3) moieties as described previously (32, 33). Oligoribonucleotides designated ARE_{xx} are variants of the core ARE sequence from TNFα mRNA (Table 1). The RNA substrate "*fos* ARE domain I" encodes a 46-nucleotide segment of the ARE from human c-*fos* mRNA that is sufficient to accelerate decay of a reporter transcript in *cis* (34). The substrate "Rβ" encodes a fragment of the coding sequence from rabbit β-globin mRNA. RNA substrate variants containing 5′-linked cyanine-3 (Cy3) or fluorescein (Fl) groups are indicated by relevant prefixes, where applicable. Similarly, RNA substrates containing 3′-fluorescein groups are suffixed by "Fl". As needed, 5′-hydroxyl RNA substrates were radiolabeled to specific activities of $3–5 \times 10^3$ cpm/fmol using T4 polynucleotide kinase and [γ-^{32}P]ATP as described previously (35).

Preparation of Recombinant AUF1 Proteins—cDNAs encoding human p42^{AUF1} and p45^{AUF1} were inserted downstream of a His_6 tag motif in pBAD/HisB (Invitrogen) using standard subcloning techniques and verified by restriction digestion and automated DNA sequencing. Construction of pBAD/HisB-based expression vectors encoding p37^{AUF1} and p40^{AUF1} was described previously (31, 36). All pBAD-HisB/AUF1 plasmids were transformed into *Escherichia coli* Ro-

setta 2 cells (Novagen), and expression of recombinant His_6-AUF1 proteins was induced with arabinose (0.02%). His_6-AUF1 proteins were purified from bacterial cell lysates by Ni^{2+}-affinity chromatography over a HiTrap chelating affinity column (GE Healthcare) essentially as described previously (36), except that after loading and washing the Ni^{2+}-affinity resin, 6 column volumes of Triton wash buffer (50 mM sodium phosphate (pH 8.0) containing 500 mM NaCl, 20 mM imidazole, and 1% Triton X-100) was also applied prior to His_6-AUF1 elution. This additional washing step improved the purity of the recovered AUF1 proteins. Proteins used for RNA-binding studies were buffer-exchanged into 10 mM Tris-HCl (pH 7.5) using a HiPrep 26/10 desalting column (GE Healthcare). For gel filtration or chemical cross-linking studies where primary amino groups must be excluded, His_6-$p37^{AUF1}$, -$p40^{AUF1}$, and -$p42^{AUF1}$ were buffer-exchanged into 10 mM HEPES-KOH (pH 7.5). Because His_6-$p45^{AUF1}$ formed significant aggregates in the HEPES buffer, a solubility screening test was performed essentially as described previously (37) to identify an optimal buffer for this isoform. 10 mM MOPS-NaOH (pH 7.5) was selected as the best buffer lacking primary amino groups among those screened based on minimization of high molecular mass complexes or aggregates as measured by dynamic light scattering using a Zetasizer nano series instrument (Malvern Instruments). All recombinant proteins were quantified by Coomassie Blue-stained SDS-PAGE against a titration of bovine serum albumin.

Gel Filtration Chromatography—A HiPrep 16/60 column (GE Healthcare) packed with Sephacryl S-200 high resolution resin was equilibrated with gel filtration buffer (10 mM HEPES-KOH (pH 7.5) containing 150 mM KCl for all isoforms except $p45^{AUF1}$, for which 10 mM MOPS-NaOH (pH 7.5) containing 150 mM KCl was used). Protein samples (140–180 μg) were diluted in gel filtration buffer (0.5 ml final volume) and centrifuged at 16,100 $\times$ *g* for 5 min to remove particulates before loading. Samples were fractionated at 30 ml/h with elution monitored by absorbance at 280 nm. Column void volume was determined using blue dextran. The column was calibrated by monitoring elution of the following protein standards (Sigma) by A_{280}: alcohol dehydrogenase (150 kDa), bovine serum albumin (66 kDa), and carbonic anhydrase (29 kDa).

Protein Cross-linking—Protein-protein cross-linking reactions (10 μl final) were assembled with His_6-AUF1 proteins (5 μM) in 10 mM HEPES-KOH (pH 7.5) containing 50 mM KCl for His_6-$p37^{AUF1}$, -$p40^{AUF1}$, and -$p42^{AUF1}$, or 10 mM MOPS-NaOH (pH 7.5) containing 50 mM KCl for His_6-$p45^{AUF1}$. Cross-linking was initiated by adding dithio-bis(succinimidyl propionate) (DSP, Thermo Scientific) dissolved in dimethyl sulfoxide (DMSO) to a final concentration of 2.5 mM. Reactions proceeded for 30 min at room temperature before quenching with 10 μl of 1 M Tris-HCl (pH 7.5) for 15 min at room temperature. Reaction products were fractionated by SDS-PAGE and detected by Western blot using anti-AUF1 antibodies (Upstate Biotechnology).

Measurements of RNA-Protein Binding—Association of recombinant AUF1 proteins with RNA substrates was qualitatively assessed using electrophoretic mobility shift assays (EMSA) essentially as described previously (38). Briefly, reactions containing limiting concentrations of ^{32}P-labeled RNA substrates (0.2 nM) and varying concentrations of protein were assembled in 10 mM Tris-HCl (pH 8) containing 50 mM KCl, 2 mM DTT, 0.5 mM EDTA, 0.1 μg/μl acetylated bovine serum albumin, 1 μg/μl heparin, and 10% glycerol (10 μl final volume). After incubating for 15 min on ice, reactions were fractionated on a 6% native acrylamide gel at 4 °C. Gels were then dried and products visualized using a PhosphorImager.

Quantitative measurement of protein-RNA-binding equilibria was performed using fluorescence anisotropy essentially as described previously (35, 36). At constant temperature and viscosity, protein binding to a fluorophore-labeled RNA increases the rotational relaxation time of the fluorophore by increasing its molecular volume and decreasing intramolecular segmental motion of the RNA substrate (39, 40). Binding reactions were assembled as described for EMSA, except that Fl-labeled RNA was employed in place of the radiolabeled substrate, total volume was 100 μl, and glycerol was omitted. After a 1-min incubation at 25 °C, fluorescence anisotropy of the Fl-RNA substrates was measured using a Beacon 2000 fluorescence polarization system (Panvera) equipped with fluorescein excitation (490 nm) and emission (535 nm) filters. Preliminary on-rate studies demonstrated that binding equilibrium was achieved for all AUF1 isoforms within this time frame (Refs. 31, 35 and data not shown). Concomitant with fluorescence anisotropy, total fluorescence emission from each reaction was also measured to verify that protein binding did not significantly alter the fluorescence quantum yields of RNA substrates (data not shown).

Binding constants describing AUF1 association with RNA substrates were resolved by nonlinear regression of total measured anisotropy as a function of protein concentration using PRISM version 3.03 software (GraphPad). Based on our interpretation of all AUF1 isoforms as dimers in solution (described under "Results"), association of a single protein dimer (P_2) to a Fl-labeled RNA substrate under limiting RNA concentrations (*i.e.*, where $[P_2]_{free} \approx [P_2]_{total}$) and constant fluorescence quantum yield is described by Equation 1.

$$A_t = \frac{A_R + A_{P2R}K[P_2]}{1 + K[P_2]} \quad \text{(Eq. 1)}$$

Here, A_t is the total measured anisotropy; A_R and A_{P2R} represent the intrinsic anisotropy of the free RNA and dimer-bound RNA substrate, respectively, and K is the apparent equilibrium association constant ($K = 1/K_d$). Equation 1 can be expanded to describe sequential two-step association of AUF1 dimers with an RNA substrate yielding tetrameric protein complexes by incorporating terms representing the intrinsic anisotropy of the protein tetramer·Fl-RNA complex (A_{P4R}) and tandem apparent association constants K_1 and K_2 in Equation 2 (35, 40).

$$A_t = \frac{A_R + A_{P2R}K_1[P_2] + A_{P4R}K_1K_2[P_2]^2}{1 + K_1[P_2] + K_1K_2[P_2]^2} \quad \text{(Eq. 2)}$$

Reactions best described by cooperative binding were resolved by a variant of the Hill model in Equation 3 where A_{PxR}

represents the intrinsic anisotropy of the saturated protein·Fl-RNA complex; $[P_2]_{½}$ is the concentration of His_6-AUF1 dimers giving half-maximal binding, and h represents the degree of cooperativity.

$$A_t = A_R + (A_{PxR} - A_R) \times \left[\frac{([P_2]/[P_2]_{1/2})^h}{1 + ([P_2]/[P_2]_{1/2})^h} \right] \quad \text{(Eq. 3)}$$

The appropriateness of each binding model was evaluated by the coefficient of determination (R^2) from individual experiments and analysis of residual plot nonrandomness to detect any bias for data subsets (PRISM). When multiple models were considered for a common data set, pairwise comparisons of sum-of-squares deviations were performed using the F test (PRISM), with differences exhibiting $p < 0.05$ considered significant.

Macromolecular Binding Density Analysis—The apparent site size of AUF1 dimer binding on an Fl-RNA substrate and the fractional contributions of each binding step to changes in its fluorescence anisotropy were resolved using macromolecular binding density analysis (MBDA). This method quantifies the degree of binding ($\sum\nu$, defined as the population-averaged number of AUF1 dimers bound per Fl-labeled RNA substrate) and free AUF1 dimer concentration ($[P_2]_F$) without any prior knowledge or assumptions regarding their relationship to the observed anisotropy signal change (ΔA_{obs}). Described in greater detail elsewhere (41, 42), MBDA presumes that every complex i containing an Fl-labeled RNA contributes to ΔA_{obs} at a given point in the titration, where $\Delta A_{obs} = A_i - A_R$, and A_R is the experimentally determined anisotropy of Fl-RNA in the absence of protein. Thus, if each i complex has a maximal per mol contribution ΔA_i to the anisotropy, the experimentally observable signal ΔA_{obs} is related to $\sum\nu$ by Equation 4.

$$\Delta A_{obs} = \sum \nu \Delta A_i \quad \text{(Eq. 4)}$$

In other words, the total signal is the population-weighted sum of contributions of the per mol anisotropy for each species i. Accordingly, the same value of ΔA_{obs} obtained at two different total RNA concentrations, $[R]_{T1}$ and $[R]_{T2}$, must be in the same physical state with the same average degree of binding $\sum\nu$ and free concentration of protein $[P_2]_F$ at the corresponding total protein concentrations, $[P_2]_{T1}$ and $[P_2]_{T2}$. Therefore, the paired ($[P_2]_T$, $[R]_T$) concentrations obtained at a point from each isotherm possessing the same ΔA_{obs} can be plotted to obtain the average binding density and free protein dimer concentration as the slope and vertical intercept, respectively, of $[P_2]_T$ *versus* $[R]_T$ by Equations 5 and 6, where $x = 1$ or 2.

$$\sum \nu = \frac{[P_2]_{T2} - [P_2]_{T1}}{[R]_{T2} - [R]_{T1}} \quad \text{(Eq. 5)}$$

$$[P_2]_F = [P_2]_{Tx} - (\sum\nu)[R]_{Tx} \quad \text{(Eq. 6)}$$

In this study, we analyzed isotherms across three RNA concentrations to obtain an estimate of the errors associated with $\sum\nu$ and $[P_2]_F$. To minimize the influence of a nonspecific binding component that contributes to ΔA_{obs} at high protein concentrations, MBDA was limited to binding data corresponding to $\Delta A_{obs} < 70 - 80\%$ of the asymptotic maximum (ΔA_{sat}) for each anisotropy isotherm. The intersection of the linearly extrapolated limiting slopes of the two binding regimes observed for ΔA_{obs} *versus* $\sum\nu$ was used to calculate $\sum\nu_{int}$, the AUF1 dimer:RNA stoichiometry that demarks a clear transition in the average anisotropic contribution with increasing binding density. The apparent site size for this intermediate complex was then estimated as the ratio of the RNA nucleotide length (N) and the intermediate stoichiometry as $n = N/\sum\nu_{int}$.

Assays of RNA Folding Using Steady State FRET—RNA remodeling by each AUF1 isoform was monitored by changes in the distance between 3′-Fl (donor) and 5′-Cy3 (acceptor) groups appended to the termini of RNA substrates using FRET, essentially as described previously (43). Briefly, FRET efficiency (E_{FRET}) varies inversely with the scalar distance (r) between a fluorescent donor (in this case Fl) and an appropriate acceptor (Cy3) by Equation 7.

$$E_{FRET} = \frac{R_0^6}{R_0^6 + r^6} \quad \text{(Eq. 7)}$$

The Förster distance (R_0) is calculable from fluorophore spectral data and represents the separation between donor and acceptor yielding $E_{FRET} = 0.5$ (44). For Fl and Cy3 dyes appended to single-stranded nucleic acids, R_0 has been calculated as 55.7 Å (45).

Varying concentrations of specified AUF1 isoforms were incubated with RNA substrates ARE_{38}-Fl (donor alone) or Cy3-ARE_{38}-Fl (donor-acceptor pair) as described for anisotropy analyses (see above), except that final RNA concentrations were 2 nM. Fluorescence from the FRET donor (Fl) was measured using a Cary Eclipse fluorometer (Varian) equipped with a sub-microcell cuvette ($\lambda_{ex} = 485$ nm, $\lambda_{em} = 520$ nm, 10-nm slit widths). Background fluorescence was quantified from samples lacking RNA substrates. Inner filter effects and photobleaching were insignificant in these experiments (data not shown). E_{FRET} between donor and acceptor fluorophores was calculated using Equation 8 (derived from Ref. 43), where $F_{Cy\text{-}Fl}$ is the background-corrected fluorescence of the donor in the presence of the acceptor (measured from the Cy-ARE_{38}-Fl substrate), F_{Fl} is the background-corrected donor fluorescence from parallel reactions lacking the acceptor (measured using the ARE_{38}-Fl substrate), and f_{DA} is the fractional labeling of the Cy3 acceptor on the Cy-ARE_{38}-Fl RNA.

$$E_{FRET} = 1 - \left[\frac{F_{Cy\text{-}Fl} - F_{Fl}(1 - f_{DA})}{F_{Fl} \cdot f_{DA}} \right] \quad \text{(Eq. 8)}$$

Correlating AUF1-dependent changes in RNA conformation with formation of specific AUF1·RNA complexes required estimation of the relative concentration of each RNA·protein complex across titrations of protein. These fractional distributions were calculated using the sequential two-step association model (described above); however, the elevated concentrations of RNA substrates required for FRET measurements necessitated consideration of protein depletion, which becomes significant at low total protein concentrations. By conservation of mass, the two-step association

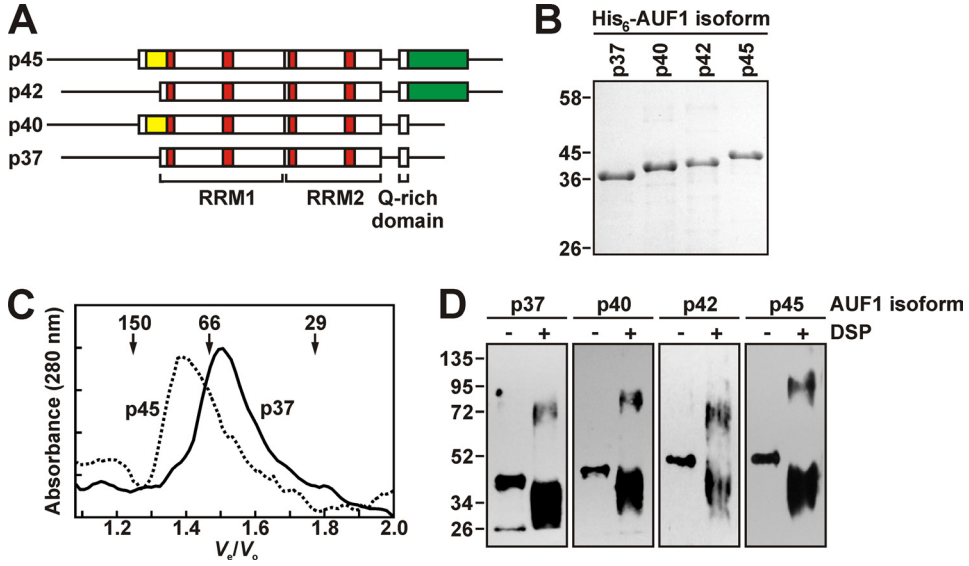

FIGURE 1. **Organization and oligomeric status of AUF1 isoforms.** *A*, all AUF1 isoforms contain tandem RNA recognition motifs that include characteristic RNP-2 and RNP-1 motifs (*red boxes*) and a downstream Gln-rich domain. The positions of isoform-specific sequences encoded by exon 2 (*yellow*) and exon 7 (*green*) are shown. *B*, purified recombinant His_6-AUF1 proteins were separated by SDS-PAGE and stained with Coomassie Blue. The migration of molecular mass markers is indicated at *left* (in kDa). *C*, representative elution profiles of His_6-$p37^{AUF1}$ (*solid line*) and His_6-$p45^{AUF1}$ (*dotted line*) fractionated through a Sephacryl S-200 gel filtration column. *Arrows* at *top* show the positions of elution peaks for protein standards (given in kDa). *D*, products generated by DSP-directed covalent cross-linking of recombinant AUF1 isoforms were separated by SDS-PAGE and identified by Western blot. A sample of untreated His_6-AUF1 (12.5% mol ratio *versus* DSP-treated sample) was run next to each cross-linking reaction to show the migration of unmodified protein. The migration of molecular mass markers is indicated at *left* (in kDa). Independent replicate experiments yielded similar results.

model requires that the total AUF1 dimer ($[P_2]_T$) and RNA ($[R]_T$) concentrations be distributed between the free ($[P_2]_F$, $[R]_F$), the single dimer-bound mode ($[P_2R]$), or the tetramer-bound mode ($[P_4R]$) by Equations 9 and 10.

$$[P_2]_T = [P_2]_F + [P_2R] + 2[P_4R] \quad \text{(Eq. 9)}$$

$$[R]_T = [R]_F + [P_2R] + [P_4R] \quad \text{(Eq. 10)}$$

The concentration of each bound species is related to $[P_2]_F$ and $[R]_F$ through the known apparent binding constants K_1 and K_2 by Equations 11 and 12, whereas the concentration of free RNA substrate can be calculated using Equation 13.

$$[P_2R] = K_1[P_2]_F[R]_F \quad \text{(Eq. 11)}$$

$$[P_4R] = K_1K_2[P_2]_F^2[R]_F \quad \text{(Eq. 12)}$$

$$[R]_F = \frac{[R]_T}{1 + K_1[P_2]_F + K_1K_2[P_2]_F^2} \quad \text{(Eq. 13)}$$

However, solution of each function requires an explicit value for $[P_2]_F$. This was calculated by combining Equations 9–13 to generate Equation 14.

$$[P_2]_T + (K_1([P_2]_T - [R]_T) - 1)[P_2]_F + (K_1K_2([P_2]_T - 2[R]_T) - K_1)[P_2]_F^2 - K_1K_2[P_2]_F^3 = 0 \quad \text{(Eq. 14)}$$

The one physically relevant cubic root for $[P_2]_F$ (*i.e.* $0 < [P_2]_F \leq [P_2]_T$) for each given $[P_2]_T$ was determined via the FindRoots operation in Igor Pro 6.1 (Wavemetrics), which was then used to solve for the fractional concentration of each AUF1·RNA complex relative to $[R]_T$ using Equations 11–13.

RESULTS

All AUF1 Isoforms Form Complexes Consistent with Dimers in the Absence of RNA—All recombinant His_6-AUF1 proteins produced using the pBAD/His vector system and purified by Ni^{2+}-affinity chromatography yielded proteins of expected molecular weights and >95% purity by SDS-PAGE (Fig. 1*B*). Previous gel filtration and analytical ultracentrifugation studies showed that $p37^{AUF1}$ is a dimer in solution and suggested that N-terminal sequences common to all isoforms were responsible for AUF1 dimerization (22). Chemical cross-linking similarly demonstrated that $p37^{AUF1}$ formed dimers in the absence of high affinity RNA substrates (35). Subsequently, glutathione *S*-transferase pulldown experiments indicated that recombinant versions of all AUF1 isoforms could form protein-protein interactions with one another (46), although the overall size of these complexes was not defined.

To determine whether all AUF1 isoforms formed dimers in solution similar to those described for $p37^{AUF1}$, two experiments were performed. First, recombinant forms of each AUF1 isoform were individually fractionated on a size-exclusion column. No distinct peaks were observed at elution volumes predicted for monomeric proteins (Fig. 1*C*). The major elution peaks for both His_6-$p40^{AUF1}$ and His_6-$p45^{AUF1}$ corresponded to apparent molecular weights twice those of each monomer, consistent with these proteins eluting as dimers (Table 2). The apparent molecular weights of His_6-$p37^{AUF1}$ and His_6-$p42^{AUF1}$ were significantly greater than those of monomers, although somewhat less than those calculated for protein dimers. Because His_6-$p37^{AUF1}$ had already been characterized as a dimer by analytical ultracentrifugation (22) and chemical cross-linking (35), our data suggest that His_6-

p37^{AUF1} and His$_6$-p42^{AUF1} are likely eluting as higher mobility dimers. It is possible that the absence of exon 2-encoded sequences in these isoforms confers distinct conformational features that alter their hydrodynamic properties. No larger oligomeric forms were detected for any AUF1 isoform in the absence of RNA. In a second series of experiments, AUF1 dimerization was tested using the chemical cross-linker DSP. All DSP-treated His$_6$-AUF1 proteins yielded products consistent with both intramolecular (Fig. 1*D*, *bottom bands*) and intermolecular (Fig. 1*D*, *top bands*) cross-links, the latter migrating with apparent molecular weights predicted for dimeric proteins. The efficiency of intermolecular cross-linking could not be directly assessed in these experiments because DSP treatment significantly weakened binding of all recombinant AUF1 proteins to anti-AUF1 antibodies or Coomassie Blue-based stains (data not shown). However, the comparable distributions of cross-linked products observed for His$_6$-p40^{AUF1}, His$_6$-p42^{AUF1}, and His$_6$-p45^{AUF1} relative to His$_6$-p37^{AUF1}, which was previously characterized as a dimer, suggest that all AUF1 isoforms are similarly dimeric in solution.

Alternatively Expressed Domains of AUF1 Regulate Both RNA-binding Affinity and RNA-induced Protein Oligomerization—Previously, we showed that two dimers of p37^{AUF1} can sequentially bind the ARE from TNFα mRNA (Fig. 2*A*) to first form a protein dimer·RNA (P_2R) complex, followed by a protein tetramer·RNA (P_4R) complex (35, 36). Using EMSAs, we observed that the other AUF1 isoforms also bind this RNA substrate in two stages, consistent with the p37^{AUF1} model (Fig. 2*B*). The faster migrating complex (complex I) is observed at lower protein concentrations, consistent with the initial protein dimer binding event (P_2R), whereas a slower mobility band appearing at higher AUF1 concentrations (complex II) is consistent with the P_4R complex. These binding events are RNA sequence-specific, because no complexes were detected in EMSAs using the Rβ RNA substrate, which lacks AU-rich sequences (data not shown). Comparing the protein concentration dependence of RNA binding among all isoforms yielded two interesting observations. First, formation of complex I required higher protein concentrations for AUF1 isoforms containing sequences encoded by exon 2 relative to their respective exon 2-deficient isoforms (Fig. 2*B*, *cf.* His$_6$-p40^{AUF1} *versus* His$_6$-p37^{AUF1} and His$_6$-p45^{AUF1} *versus* His$_6$-p42^{AUF1}), suggesting that the inclusion of exon 2-encoded sequences inhibits formation of the initial AUF1·RNA P_2R complex. Second, complex II assembly was observed at lower protein concentrations for AUF1 isoforms that contained sequences encoded by exon 7 (Fig. 2*B*, *cf.* His$_6$-p42^{AUF1} *versus* His$_6$-p37^{AUF1} and His$_6$-p45^{AUF1} *versus* His$_6$-p40^{AUF1}), suggesting that the second binding step (*i.e.* leading to formation of the P_4R complex) might be enhanced by the exon 7-encoded domain.

TABLE 2
Gel filtration analyses of recombinant AUF1 isoforms

AUF1 isoform	Calculated mass[a]	Apparent mass[b]
	Da	*Da*
p45^{AUF1}	43,411	87,500
p42^{AUF1}	41,248	64,300
p40^{AUF1}	37,811	72,900
p37^{AUF1}	35,648	61,600

[a] Data were calculated using the AASTATS tool at the San Diego Supercomputer Center Biology Workbench, using human AUF1 protein sequences appended to the vector-encoded N-terminal His$_6$ tag and Xpress epitope- (GenBank^{TM} accession numbers: p45^{AUF1}, NP_112738; p42^{AUF1}, NP_112737; p40^{AUF1}, NP_002129; and p37^{AUF1}, NP_001003810).
[b] Data were resolved by gel filtration chromatography as described under "Experimental Procedures."

To quantitatively assess recombinant His$_6$-AUF1 binding to RNA targets, we measured the change in fluorescence anisotropy of the Fl-ARE$_{38}$ substrate as a function of protein concentration. As reported previously (31, 36), His$_6$-p37^{AUF1} (Fig. 3*A*) and His$_6$-p40^{AUF1} (data not shown) binding to this RNA target was well described by the two-step sequential binding model of Equation 2, permitting explicit solutions of binding constants describing both stages of RNP assembly (Table 3). Appropriateness of the two-step binding model was supported by random distributions of residuals (*e.g.* Fig. 3*A*, *bottom*) and high coefficients of determination ($R^2 > 0.98$) across

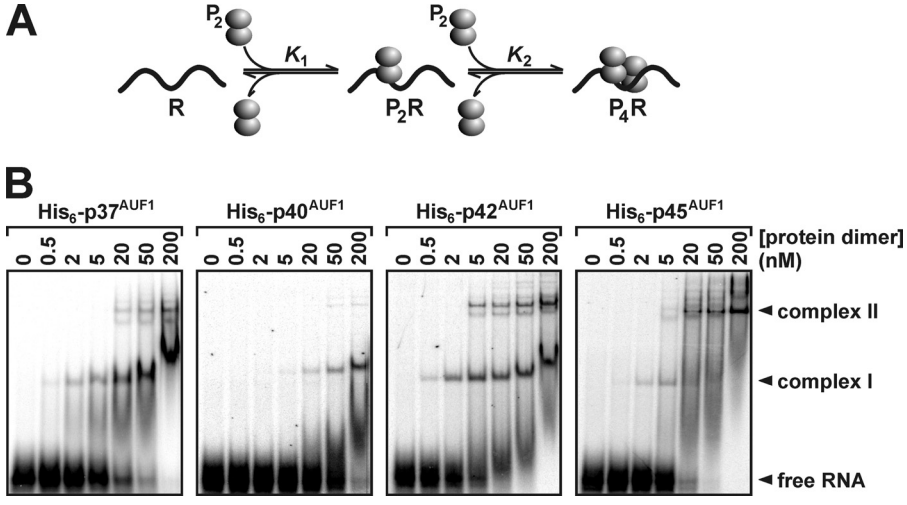

FIGURE 2. **Evaluation of His$_6$-AUF1 binding to the ARE$_{38}$ RNA substrate by EMSA.** *A*, sequential dimer association model for AUF1 binding to an RNA substrate. *B*, binding reactions containing a 5′-^{32}P-labeled ARE$_{38}$ RNA substrate, and titrations of each recombinant His$_6$-AUF1 isoform were assembled as described under "Experimental Procedures" prior to fractionation on nondenaturing gels. Bands corresponding to distinct RNA·protein complexes formed on the ^{32}P-ARE$_{38}$ substrate are indicated as *complexes I* and *II*. Unbound probe is designated as *free RNA*.

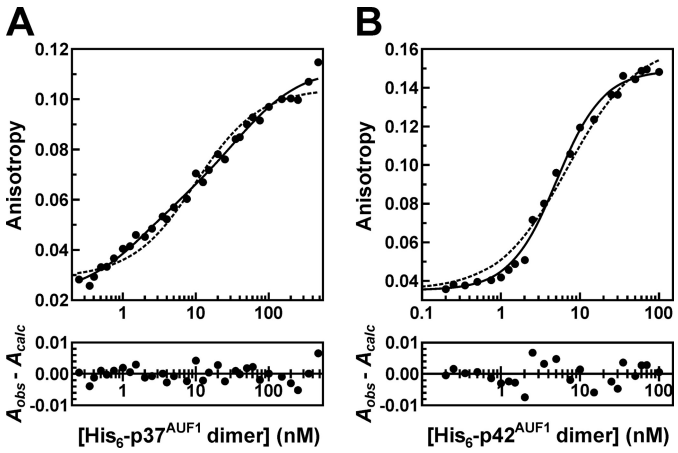

FIGURE 3. **Analysis of His_6-AUF1 binding to the Fl-ARE_{38} RNA substrate using fluorescence anisotropy.** The fluorescence anisotropy of reactions containing the Fl-ARE_{38} RNA substrate (0.2 nM) and varying concentrations of recombinant His_6-p37^{AUF1} (*A*) or His_6-p42^{AUF1} (*B*) was measured as described under "Experimental Procedures." His_6-p37^{AUF1} binding to this RNA substrate was resolved by the sequential two-step binding algorithm (Equation 2), although His_6-p42^{AUF1} binding required a cooperative binding model (Equation 3) (*solid lines*). Constants describing regression solutions are listed in Table 3. For comparison, optimal fits to single-site binding models (Equation 1) are also shown for each dataset (*dotted lines*). Residual plots show random deviation of the preferred binding models (A_{calc}) from observed data (A_{obs}) (*lower panels*).

TABLE 3

Affinity of recombinant AUF1 isoforms for the Fl-ARE_{38} RNA substrate

Apparent dissociation constants were solved for each binding step of His_6-p37^{AUF1} and His_6-p40^{AUF1} on the Fl-ARE_{38} substrate by resolving association constants K_1 and K_2 from anisotropy isotherms (*e.g.* Fig. 3) using Equation 2, which were then converted using $K_d = 1/K$. For His_6-p42^{AUF1} and His_6-p45^{AUF1}, the cooperative binding model of Equation 3 resolved the protein dimer concentrations yielding 50% binding ($[P_2]_{1/2}$) and the Hill coefficients (*h*). All values represent the mean ± standard deviation of *n* independent experiments.

Isoform	$K_{d1,\,app}$	$K_{d2,\,app}$	*n*
	nM	nM	
p37	1.7 ± 0.3	74 ± 16	6
p40	10 ± 2	160 ± 19	4
	$[P_2]_{½}$	*h*	
	nM		
p42	4.4 ± 0.7	1.39 ± 0.06	5
p45	14 ± 2	1.02 ± 0.02	4

all experiments. The single site binding model of Equation 1 (*e.g.* Fig. 3*A*, *dotted line*) was clearly inappropriate, as shown by significant residual nonrandomness ($p < 0.0001$) and by significant increases in the sum-of-squares deviations when compared with regression solutions based on the two-step binding model using the *F* test ($p < 0.0001$). By contrast, binding of His_6-p42^{AUF1} and His_6-p45^{AUF1} to the Fl-ARE_{38} substrate could not be confidently resolved using Equation 2 because of redundancy in fitting the A_{P2R} and K_2 parameters. This frequently occurs for data sets where K_1 and K_2 vary by less than 5-fold and prevents explicit solution of binding constants using this approach when the value of A_{P2R} is unknown (40). However, the protein concentration dependence of His_6-p42^{AUF1} (Fig. 3*B*) and His_6-p45^{AUF1} (data not shown) binding to the Fl-ARE_{38} substrate was well described using the cooperative binding model of Equation 3. Resolution of *h* significantly greater than 1 for His_6-p42^{AUF1} binding to this RNA substrate (Table 3) suggests that binding may be cooperative, with the second dimer binding more strongly than the first. This possibility is dependent on the intrinsic anisotropy of the protein dimer-bound RNA complex (A_{P2R} from Equation 2) and is addressed further below. Analyses of His_6-p45^{AUF1} association with the Fl-ARE_{38} substrate using Equation 3 resolved $h \approx 1$, indicating that both protein binding steps are likely to be thermodynamically similar.

Comparing the binding constants describing the association of each His_6-AUF1 isoform with the Fl-ARE_{38} substrate supports independent roles for domains encoded by alternatively spliced exons of AUF1. First, constants describing His_6-p37^{AUF1} and His_6-p40^{AUF1} binding to the Fl-ARE_{38} substrate show that the presence of exon 2-encoded sequences in His_6-p40^{AUF1} inhibits the first RNA-binding event by nearly 6-fold and the second binding event by ~2-fold relative to the p37 isoform (Table 3). Although EMSAs from this (Fig. 2*B*) and previous studies (20) indicated that p40^{AUF1} binds ARE substrates more weakly than p37^{AUF1}, the anisotropy-based experiments show that this distinction is principally manifested at the initial contact with the RNA substrate. However, the anisotropy-based binding assays also revealed a novel effect of exon 7-encoded sequences on the assembly of AUF1 RNPs, involving dramatic enhancement of the second binding step. Although a His_6-p37^{AUF1} dimer binds to the P_2R complex on the Fl-ARE_{38} substrate with a modest apparent K_d of 74 nM based on the two-step binding model (Equation 2), the potential cooperativity of His_6-p42^{AUF1} binding to this substrate shown by Hill analysis (Equation 3) indicates that the affinity of the second binding step is near or better than the $[P_2]_{½}$ value of 4.4 nM (Table 3). Similarly, the second His_6-p40^{AUF1} dimer is recruited very weakly with an apparent K_d of 160 nM, although inclusion of exon 7-encoded sequences (yielding His_6-p45^{AUF1}) improves the affinity of this step to ~14 nM, the $[P_2]_{½}$ value for His_6-p45^{AUF1} binding to the Fl-ARE_{38} substrate. Together with the protein concentration dependence of binding described by EMSAs (Fig. 2*B*), our anisotropy-based binding studies show that the AUF1 protein domain encoded by exon 7 enhances formation of AUF1 oligomers on the TNFα ARE by improving the affinity of the second dimer binding event, although sequences encoded by exon 2 can inhibit AUF1 recruitment to the ARE substrate by weakening the affinity of the first binding step.

Enhanced ARE-induced AUF1 Oligomerization Regulated by Exon 7-encoded Sequences Does Not Result from Variations in Binding Site Size—Although our binding studies show that the exon 7-encoded sequences near the C terminus of His_6-p42^{AUF1} and His_6-p45^{AUF1} enhance assembly of protein tetramers on the TNFα ARE substrate, it is not known how this domain promotes binding of the second AUF1 dimer. Conceivably, this domain may participate in protein-protein contacts or may direct conformational events that enhance the second binding step. Alternatively, the RNA-binding site for AUF1 isoforms lacking exon 7-encoded sequences may be too large to permit multiple high affinity binding events on the 38-nucleotide TNFα ARE substrate. In the latter case, high affinity recruitment of the second His_6-p37^{AUF1} or His_6-p40^{AUF1} dimer might be precluded simply because an insufficient length of RNA is presented to the protein.

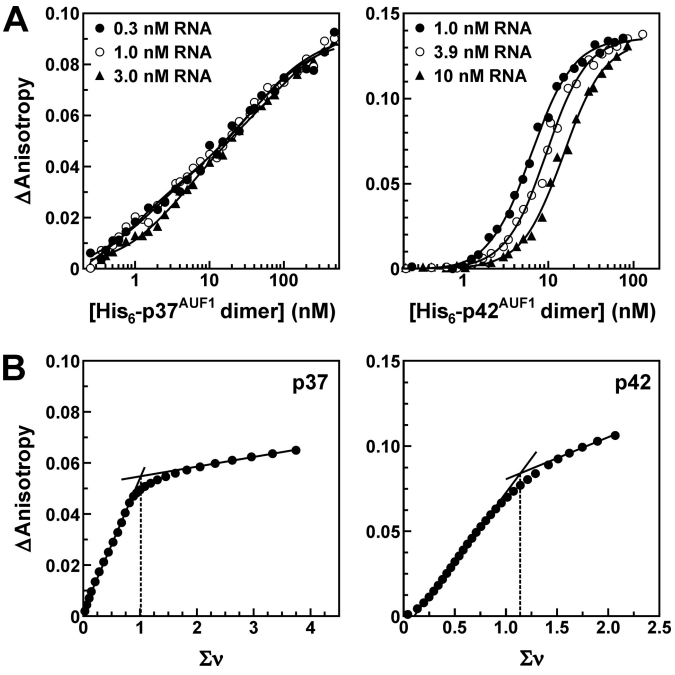

FIGURE 4. **MBDA of His_6-$p37^{AUF1}$ and His_6-$p42^{AUF1}$ binding to the Fl-ARE_{38} RNA substrate.** *A*, fluorescence anisotropy-based assays of His_6-$p37^{AUF1}$ (*left*) or His_6-$p42^{AUF1}$ (*right*) binding to the Fl-ARE_{38} substrate under conditions of varying RNA substrate concentrations. *Solid lines* represent nonlinear least squares fits to either the two-step sequential dimer binding model for His_6-$p37^{AUF1}$ (Equation 2) or the cooperative binding model for His_6-$p42^{AUF1}$ (Equation 3). *B*, changes in observed anisotropy (ΔA_{obs} in Equation 4) plotted as a function of the ensemble-averaged number of His_6-$p37^{AUF1}$ (*left*) or His_6-$p42^{AUF1}$ (*right*) dimers bound per RNA strand ($\sum\nu$), calculated as described under "Experimental Procedures." *Solid lines* represent the limiting slopes corresponding to the low and high affinity binding phases. The *dotted vertical lines* indicate the stoichiometry of the AUF1·RNA complex where the low binding density phase transitions into the high binding density regime ($\sum\nu = 1.02 \pm 0.02$ for His_6-$p37^{AUF1}$ and $\sum\nu = 1.14 \pm 0.06$ for His_6-$p42^{AUF1}$).

TABLE 4

ARE substrate length requirements for association and oligomerization of $p37^{AUF1}$

RNA substrate	$K_{d1,\,app}$ [a]	$K_{d2,\,app}$ [a]	*n*
	nM	*nM*	
Fl-ARE_{44}	2.2 ± 0.1	63 ± 7	3
Fl-ARE_{38}	1.7 ± 0.3	74 ± 16	6
Fl-ARE_{35}	3.2 ± 0.3	130 ± 20	3
Fl-ARE_{34}	3.0 ± 0.3	117 ± 6	3
Fl-ARE_{30}	7.0 ± 0.4	>600	3
Fl-ARE_{24}	26 ± 2	NA[b]	3
Fl-ARE_{20}	33 ± 3	NA	3
Fl-ARE_{18}	69 ± 12	NA	4

[a] Apparent equilibrium dissociation constants describing the first ($K_{d1,\,app}$) and second ($K_{d2,\,app}$) stages of His_6-$p37^{AUF1}$ dimer binding to Fl-labeled RNA substrates were resolved from anisotropy plots using the two-step binding model of Equation 2 as described in Table 3. For RNA substrates ≤24 bases in length, the second protein dimer binding event was not detectable. In these cases, simplification of Equation 2 with $K_{d2,\,app} = 0$ yields Equation 1, giving the apparent bimolecular dissociation constant for the initial binding event only. All constants are expressed as the mean ± S.D. for *n* independent experiments.

[b] NA means not applicable.

TABLE 5

ARE substrate length requirements for association and oligomerization of $p42^{AUF1}$

RNA substrate	$[P_2]_{½}$ or $K_{d2,\,app}$ [a]	h^a	*n*
	nM		
Fl-ARE_{44}	4.9 ± 0.4	1.28 ± 0.04	3
Fl-ARE_{38}	4.4 ± 0.7	1.39 ± 0.06	5
Fl-ARE_{35}	6.8 ± 0.5	1.16 ± 0.03	3
Fl-ARE_{34}	11.5 ± 0.2	1	3
Fl-ARE_{30}	14 ± 2	1	4
Fl-ARE_{24}	28 ± 3	1	3
Fl-ARE_{20}	33 ± 4	1	3
Fl-ARE_{18}	106 ± 22	1	4

[a] The concentration of His_6-$p42^{AUF1}$ dimers yielding half-maximal binding ($[P_2]_{½}$) to Fl-labeled RNA substrates and associated Hill coefficients (*h*) were calculated from A_t *versus* [His_6-$p42^{AUF1}$ dimer] anisotropy plots (*e.g.* Fig. 3*B*) using Equation 3. For RNA substrates ≤34 bases in length, the Hill coefficient did not significantly differ from unity. In these cases, solution of Equation 3 with $h = 1$ yielded apparent bimolecular dissociation constants ($K_{d,\,app}$). All constants are expressed as the mean ± S.D. across n independent experiments.

To distinguish these possibilities, we assessed the influence of the exon 7-encoded domain of AUF1 on apparent RNA-binding site size by performing macromolecular binding density analysis (MBDA; described in Refs. 41, 47) of His_6-$p37^{AUF1}$ and His_6-$p42^{AUF1}$ on the Fl-ARE_{38} RNA substrate. Fluorescence anisotropy isotherms were collected across titrations of His_6-$p37^{AUF1}$ and His_6-$p42^{AUF1}$ using three different RNA substrate concentrations. The isotherms shift to the right with increasing RNA concentration because more protein is required to reach an equivalent degree of RNA saturation, reflected by the change in anisotropy (Fig. 4*A*). MBDA was performed using these anisotropy isotherms as described under "Experimental Procedures." For both His_6-$p37^{AUF1}$ and His_6-$p42^{AUF1}$, changes in Fl-ARE_{38} anisotropy as a function of the population-averaged number of AUF1 dimers bound per Fl-ARE_{38} RNA substrate ($\sum\nu$) clearly show nonlinear behavior, indicating the presence of at least two binding phases (Fig. 4*B*). The intersection obtained by linearly extrapolating the limiting slopes of the two binding regimes quantifies the AUF1:Fl-ARE_{38} stoichiometry where the transition occurs (Fig. 4*B*, *dotted lines*). This binding transition occurs at $\sum\nu \sim 1$ for both His_6-$p37^{AUF1}$ and His_6-$p42^{AUF1}$, suggesting that the low binding density phase reflects the progress of one AUF1 dimer binding to Fl-ARE_{38}, whereas the second binding regime describes subsequent AUF1 oligomerization processes. Based on the diversity of RNA sequences targeted by AUF1 (25, 48–51) and the repetitive AU-rich motifs within the Fl-ARE_{38} substrate (Table 1), we considered elements targeted by AUF1 within this RNA as a quasi-homogeneous lattice of sites. Accordingly, the binding density at the transition between binding regimes provides an estimate of the RNA site size for the low binding density complex (52) based on $n = 38/\sum\nu$ for the 38-nt Fl-ARE_{38} RNA, yielding apparent site sizes of 34 ± 2 nt for His_6-$p37^{AUF1}$ and 33 ± 2 nt for His_6-$p42^{AUF1}$ on this RNA substrate.

The apparent RNA site sizes for His_6-$p37^{AUF1}$ and His_6-$p42^{AUF1}$ predicted by MBDA were independently confirmed through equilibrium binding experiments with ARE substrates of varying lengths (Table 1). Expanding the RNA target to the 44-nt Fl-ARE_{44} substrate yielded no significant changes in the affinity of His_6-$p37^{AUF1}$ (Table 4) or His_6-$p42^{AUF1}$ (Table 5), despite a 16% increase (+6 nt) in RNA length. For His_6-$p37^{AUF1}$, the apparent binding affinity of the first protein dimer ($K_{d1,\,app}$) was also unaffected by truncation of the RNA substrate to 34 nt (Table 4, *cf.* Fl-ARE_{34} and Fl-ARE_{35} *versus* Fl-ARE_{38}). However, the initial protein binding event was inhibited by over 2-fold for the 30-nt Fl-ARE substrate *versus* the Fl-ARE_{34} target and much more severely as the RNA sub-

strate was further truncated. These data indicate that 30–34 nt of ARE sequence are required for maximal His_6-$p37^{AUF1}$ binding activity, agreeing closely with the MBDA-resolved site size estimate (see above). Interestingly, the apparent affinity of the second His_6-$p37^{AUF1}$ dimer binding step ($K_{d2,\,app}$) was similarly sensitive to the length of the RNA substrate, because this binding event was extremely weak or undetectable for ARE substrates of 30 nt or less. For His_6-$p42^{AUF1}$, potential cooperativity for some RNA substrates precluded explicit solutions for individual binding constants (discussed above). However, comparison of the protein dimer concentrations required for half-maximal binding ($[P_2]_{½}$) revealed a modest decrease in affinity between the 38- and 35-mer RNA substrates (Table 5), but more pronounced diminution in His_6-$p42^{AUF1}$ binding activity for substrates of 34 nt or less. The effects of ARE length on the RNA-binding affinities of His_6-$p37^{AUF1}$ and His_6-$p42^{AUF1}$ resolved by these binding studies are completely consistent with apparent RNA site sizes resolved by MBDA (see above) and do not significantly differ for His_6-$p37^{AUF1}$ *versus* His_6-$p42^{AUF1}$. As such, isoform-dependent variations in the binding site size of the AUF1 dimer·RNA (P_2R) complex cannot account for the enhanced RNA-dependent protein oligomerization activity observed in AUF1 isoforms containing the exon 7-encoded domain.

Finally, MBDA was used to solve explicit solutions for apparent dissociation constants describing the initial ($K_{d1,\,app}$) and secondary ($K_{d2,\,app}$) His_6-$p42^{AUF1}$ dimer binding events on the Fl-ARE_{38} substrate, thus permitting quantitative comparisons of each stage of AUF1 RNP assembly. MBDA allowed individual binding constants to be resolved for His_6-$p42^{AUF1}$ because the slope of the low binding regime ($\Delta F_1 = \partial\Delta A/\partial\sum\nu$) is a quantitative measure of the average intrinsic anisotropy change resulting from a single AUF1 dimer binding to the RNA. Applied to the sequential dimer binding model of Equation 2, ΔF_1 thus provides an independent measure of the A_{P2R} parameter ($\Delta F_1 = A_{P2R} - A_R$). For example, the MBDA-determined ΔF_1 for His_6-$p37^{AUF1}$ dimer binding to the Fl-ARE_{38} substrate was 0.050 ± 0.001, equivalent to 54% of the maximal protein-induced change in anisotropy of this substrate based on $\Delta A_{max} = 0.0928$ (Fig. 4). This value is indistinguishable from the average A_{P2R} obtained from nonlinear least squares fitting of His_6-$p37^{AUF1}$ titrations using the sequential dimer binding model of Equation 2, where ΔA_{P2R} ($=A_{P2R} - A_R$) was 52 ± 4% of ΔA_{max} across six independent protein titrations (*e.g.* Figs. 3*A* and 4*A*). For His_6-$p42^{AUF1}$ binding the Fl-ARE_{38} substrate, MBDA resolved $\Delta F_1 = 81 \pm 1$ mA, equivalent to 60% of ΔA_{max}. Applying this value as the fractional amplitude of the first binding event in the sequential dimer binding model of Equation 2 revealed that His_6-$p42^{AUF1}$ dimers bind this RNA target with $K_{d1,\,app} = 6.6 \pm 1.1$ nM and $K_{d2,\,app} = 3.8 \pm 0.9$ nM ($n = 5$). The significantly enhanced affinity of the second dimer binding event over the first ($p = 0.0022$ *versus* $K_{d1,\,app}$) affirms that His_6-$p42^{AUF1}$ dimers bind cooperatively to the Fl-ARE_{38} substrate. Furthermore, comparing the resolved $K_{d2,\,app}$ values for His_6-$p37^{AUF1}$ (Table 3) *versus* His_6-$p42^{AUF1}$ (above) binding to this RNA target indicates that the presence of the exon 7-encoded domain enhances the affinity of the second AUF1 dimer binding step by almost 20-fold.

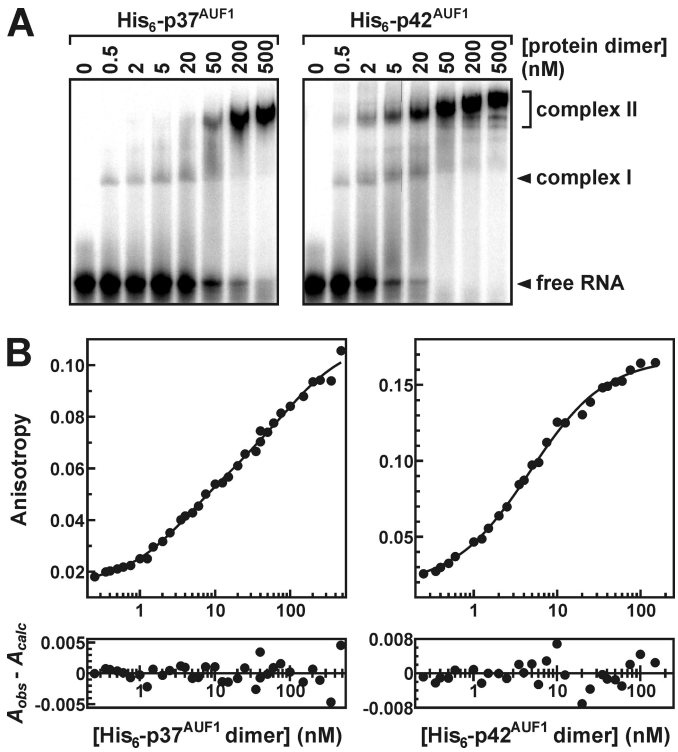

FIGURE 5. **Evaluation of His_6-AUF1 binding to the *fos* ARE domain I RNA substrate *in vitro*.** *A*, EMSAs were performed using the ^{32}P-labeled *fos* ARE domain I substrate (0.2 nM) and titrations of His_6-$p37^{AUF1}$ (*left*) or His_6-$p42^{AUF1}$ (*right*). Two distinct species resulting from protein binding to the *fos* ARE domain I substrate are indicated as *complexes I* and *II* while unbound probe is designated as *free RNA*. *B*, representative analyses of His_6-$p37^{AUF1}$ (*left*) or His_6-$p42^{AUF1}$ (*right*) binding to the Fl-*fos* ARE domain I RNA substrate by fluorescence anisotropy. Similar to the results of Fig. 3, His_6-$p37^{AUF1}$ binding to the Fl-*fos* ARE domain I RNA substrate was best resolved by the sequential two-step binding algorithm (Equation 2) and His_6-$p42^{AUF1}$ binding via the cooperative binding model (Equation 3) (*solid lines*). Averaged constants describing regression solutions from triplicate independent experiments are given in the text. Residuals plots for each binding isotherm showed no bias for data subsets (*bottom panels*).

To this point, all RNA-binding experiments were performed using the ARE from TNFα mRNA or truncated versions thereof. To determine whether exon 7-encoded sequences enhanced AUF1 oligomerization on an independent RNA substrate, we also compared the binding properties of His_6-$p37^{AUF1}$ and His_6-$p42^{AUF1}$ on the 46-nt ARE domain I fragment from c-*fos* mRNA (34). EMSAs showed that both isoforms formed two complexes on this RNA substrate in a protein concentration-dependent manner (Fig. 5*A*). Furthermore, assembly of the larger P_4R RNP (complex II) was observed at lower protein concentrations for His_6-$p42^{AUF1}$ than for His_6-$p37^{AUF1}$, consistent with the preferential formation of P_4R complexes previously described for the p42 isoform on the TNFα-based ARE_{38} substrate (Fig. 2*B*). Quantitative anisotropy-based binding experiments showed that the first His_6-$p37^{AUF1}$ dimer bound strongly to the Fl-*fos* ARE domain I substrate (Fig. 5*B*, *left*; $K_{d1,\,app} = 3.8 \pm 0.5$ nM; $n = 4$), whereas the second dimer bound much more weakly ($K_{d2,\,app} = 120 \pm 20$ nM), a relationship similar to that observed for His_6-$p37^{AUF1}$ complex assembly on the TNFα ARE.

By contrast, resolution of His_6-$p42^{AUF1}$ binding to the Fl-*fos* ARE domain I substrate required the cooperative binding model, and yielded $[P_2]_{½} = 5.6 \pm 0.8$ nM with $h = 0.96 \pm 0.04$ ($n = 3$) (Fig. 5*B*, *right*), consistent with similar binding affinities for both stages of P_4R assembly. Together, these data show that enhancement of the second AUF1 binding step by exon 7-encoded sequences is not specific for the TNFα ARE, and may apply to all AUF1 substrate RNAs.

AUF1 Isoform-dependent Effects on Local Structural Remodeling of an RNA Substrate—Previously, we used FRET to show that both His_6-$p37^{AUF1}$ and His_6-$p40^{AUF1}$ structurally condense bound RNA substrates, based on protein-induced diminution of the distance between their 5′ and 3′ termini (31, 32). In this study, we showed that AUF1 sequences encoded by exon 7 dramatically enhance the affinity of the second protein dimer binding step that leads to formation of AUF1 tetrameric complexes on RNA targets. To determine whether exon 7-encoded sequences direct unique structural consequences on AUF1-bound RNA, either promoting or as a consequence of this second binding step, we used FRET to compare protein-dependent changes in the global structure of the Cy3-ARE_{38}-Fl substrate across all AUF1 isoforms.

In the absence of protein, FRET efficiency (E_{FRET}) between the 3′-Fl and 5′-Cy3 moieties of the Cy3-ARE_{38}-Fl substrate was typically between 0.40 and 0.45 under the reaction conditions employed. Titration of His_6-$p37^{AUF1}$ led to an increase in E_{FRET} to values of 0.70 to 0.75 (Fig. 5*A*, *black line*), indicating that protein binding brings the termini of the RNA substrate closer in space. Comparing the protein concentration dependence of E_{FRET} with the fractional concentration of each fluorescent species shows that this condensation of RNA structure correlates with the initial protein dimer binding event that assembles the P_2R complex (Fig. 5*A*, *gray lines*). No significant change in E_{FRET} was observed accompanying the $P_2R \rightarrow P_4R$ transition for His_6-$p37^{AUF1}$, consistent with previous findings (32). Because the affinity of the ARE_{38} substrate for His_6-$p40^{AUF1}$ is weaker than for His_6-$p37^{AUF1}$ (Table 3), higher protein concentrations are required for the p40 isoform to drive complex assembly. However, the consequences of His_6-$p40^{AUF1}$ binding on E_{FRET} between the 5′ and 3′ termini of the Cy-ARE_{38}-Fl substrate (Fig. 6*B*) were very similar to those observed with His_6-$p37^{AUF1}$ and favor adoption of a condensed RNA conformation.

AUF1 isoforms containing the exon 7-encoded domain induced dramatically different conformations on associated RNA targets. For His_6-$p42^{AUF1}$, binding of a single protein dimer to the Cy3-ARE_{38}-Fl substrate was associated with increasing E_{FRET} (Fig. 5*C*), similar to that described for the p37 isoform. However, formation of the P_4R complex coincided with a decrease in E_{FRET}, indicating that the RNA adopts an increasingly extended conformation as the P_2R population shifts toward P_4R. In fact, within the His_6-$p42^{AUF1}$ P_4R complex the distance between the termini of the Cy3-ARE_{38}-Fl substrate is similar to that experienced by the unbound RNA, based on the similarities in E_{FRET} values. Finally, the protein concentration dependence of E_{FRET} for His_6-$p45^{AUF1}$ binding to the Cy3-ARE_{38}-Fl substrate resembled that described for His_6-$p42^{AUF1}$ binding, although the degree of RNA extension

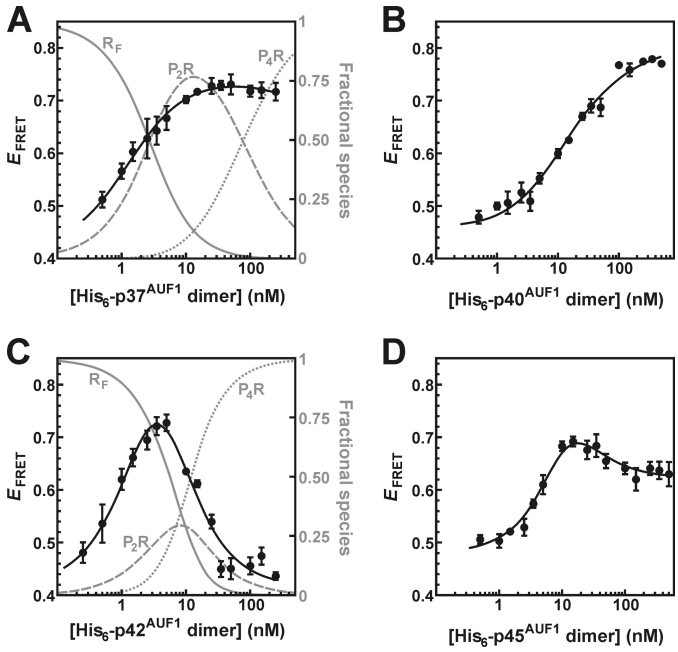

FIGURE 6. **Evaluation of RNA remodeling activities of His_6-AUF1 isoforms using FRET.** AUF1-dependent changes in the distance between the termini of an RNA substrate were determined by measuring the efficiency of FRET (E_{FRET}) from the 3′-Fl moiety to the 5′-Cy3 group of RNA substrate Cy-ARE_{38}-Fl. E_{FRET} calculations (Equation 8) were based on measurements of donor fluorescence intensity from binding reactions containing RNA substrates ARE_{38}-Fl (F_{Fl}) or Cy3-ARE_{38}-Fl ($F_{Cy\text{-}Fl}$) across a range of His_6-$p37^{AUF1}$ (*A*), His_6-$p40^{AUF1}$ (*B*), His_6-$p42^{AUF1}$ (*C*), and His_6-$p45^{AUF1}$ (*D*) concentrations. *Solid circles* represent the mean ± S.E. for at least three independent experiments. *Black lines* highlight protein concentration-dependent trends in E_{FRET} and do not denote any physical meaning. For titrations of His_6-$p37^{AUF1}$ (*A*) and His_6-$p42^{AUF1}$ (*C*), the *right vertical axis* quantifies the fractional concentrations of free RNA (*solid gray lines*), P_2R complexes (*dashed gray lines*), and P_4R complexes (*dotted gray lines*) as a function of His_6-$p37^{AUF1}$ or His_6-$p42^{AUF1}$ concentration using binding constants resolved by anisotropy experiments and fit to the sequential dimer binding model with consideration of protein depletion (Equations 11–14).

observed at high protein concentrations was much less dramatic (Fig. 6*D*). These data indicate that the RNA remodeling activities of His_6-$p45^{AUF1}$ may be intermediate to those of His_6-$p40^{AUF1}$ and His_6-$p42^{AUF1}$ and suggest that the domains encoded by exons 2 and 7 may exert distinct and possibly additive effects on the assembly of RNP complexes and the conformational fate of targeted RNA substrates.

DISCUSSION

Several features of the AUF1 family of RNA-binding proteins support the hypothesis that the individual isoforms generated by alternative pre-mRNA splicing perform distinct but possibly overlapping functions. Although all AUF1 isoforms display ARE binding activity, variations have been reported in their subcellular distribution, regulated expression, and mRNA-destabilizing roles (described under Introduction). In this study, we have quantitatively compared the RNA-binding properties of each isoform using a variety of biophysical approaches, and we have identified isoform-specific differences in RNA recognition and remodeling that may contribute to the functional and regulatory heterogeneity of these proteins.

For all AUF1 isoforms, association with model ARE substrates was consistent with sequential binding of protein

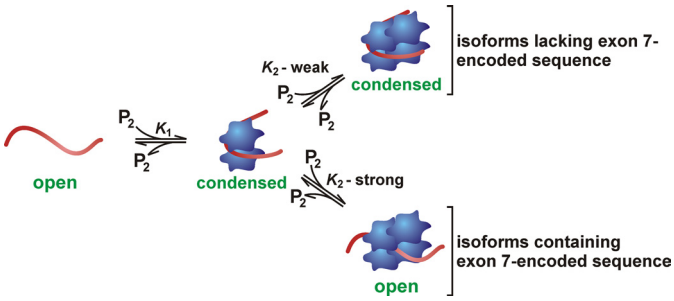

FIGURE 7. **AUF1 isoform-specific control of protein oligomerization and local RNA structure.** A schematic depicting the effects of exon 7-encoded sequences on RNP assembly by AUF1 and on the relative conformation of bound RNA substrates (described in *green*). Initial contact between any AUF1 isoform and an RNA substrate induces a condensed RNA conformation; however, sequences encoded by exon 2 (in $p40^{AUF1}$ and $p45^{AUF1}$) weaken this interaction (K_1). For AUF1 isoforms lacking exon 7-encoded sequences ($p37^{AUF1}$ and $p40^{AUF1}$), the second binding step forming the tetrameric protein·RNA complex (K_2) is relatively weak and maintains the bound RNA in a condensed conformation. By contrast, the second binding step is much stronger for AUF1 isoforms containing sequences encoded by exon 7 ($p42^{AUF1}$ and $p45^{AUF1}$) and confers a relatively open conformation on the bound RNA substrate.

dimers to generate a protein tetramer·RNA (P_4R) complex. Inclusion of sequences encoded by exon 2 (in $p40^{AUF1}$ and $p45^{AUF1}$) weakened the affinity of these binding events, in agreement with semi-quantitative EMSA-based experiments using extended ARE-containing RNA substrates (20) and single-stranded telomeric DNA sequences (51). Because the exon 2-encoded domain is contiguous with RRM1, its inclusion may alter the conformation of this RNA-binding pocket or its access to nucleic acid substrates. Although exon 2-encoded sequences significantly inhibited RNA-binding affinity, FRET experiments of RNA folding suggested that this domain likely had little effect on the conformation of bound RNA substrates. By contrast, the domain encoded by exon 7 exerted profound effects on both the energetics of AUF1 RNP assembly and the structural consequences of the associated RNA. Initial binding of all AUF1 isoforms with the ARE_{38} substrate yielded a P_2R complex containing a conformationally condensed RNA (Fig. 7). However, protein isoforms containing exon 7-encoded sequences ($p42^{AUF1}$ and $p45^{AUF1}$) displayed much stronger affinity at the second binding step (K_2), which in the case of $p42^{AUF1}$ resulted in cooperative binding to the ARE_{38} substrate. Furthermore, the ARE substrate within $p42^{AUF1}$- or $p45^{AUF1}$-containing P_4R complexes presented a less compact conformation than RNPs containing exon 7-deficient AUF1 isoforms (Fig. 6).

Although the mechanistic basis for enhanced protein oligomerization on ARE substrates by $p42^{AUF1}$ or $p45^{AUF1}$ remains unknown, several observations suggest that the exon 7-encoded domain directs unique conformational events during RNP assembly. First, AUF1 isoforms containing exon 7-encoded sequences exert greater rotational restriction on the 5′-Fl groups of RNA substrates in the P_4R complex than AUF1 proteins lacking this domain. For example, formation of the P_4R complex with His_6-$p37^{AUF1}$ increased the fluorescence anisotropy of the Fl group on the 5′-end of the ARE_{38} substrate by 0.093 ± 0.002 relative to the free RNA (Fig. 3*A*). By contrast, the His_6-$p42^{AUF1}$ P_4R complex increased the anisotropy of this fluorophore by 0.134 ± 0.001 (Fig. 3*B*). Similar differences were observed comparing His_6-$p40^{AUF1}$ *versus* His_6-$p45^{AUF1}$ binding to the Fl-ARE_{38} substrate (data not shown) and among His_6-$p37^{AUF1}$ *versus* His_6-$p42^{AUF1}$ P_4R complexes on the Fl-*fos* ARE domain I RNA substrate (Fig. 5*B*). Second, the apparent RNA site size of an AUF1 dimer is unaffected by the presence of the exon 7-encoded domain (Fig. 4 and associated text), indicating that ARE substrates do not present more high affinity sites to AUF1 isoforms containing sequences encoded by exon 7. Finally, the exon 7 domain-dependent effects of AUF1 on RNA substrate conformation in the P_4R complex (Fig. 6) indicate a direct consequence of this alternatively expressed domain on RNP architecture. Intriguingly, a recent report indicates that the splicing repressor hnRNP A1 can also bind cooperatively to RNA substrates (53). Although hnRNP A1 and AUF1 share many common features, there is no sequence in hnRNP A1 orthologous to the exon 7-encoded domain of AUF1 (supplemental Fig. 1), suggesting that a distinct biochemical mechanism is likely involved in cooperative assembly of hnRNP A1·RNA complexes.

The AUF1 isoform-dependent conformational remodeling of RNA substrates demonstrated in this work highlights an emerging theme of reciprocal interplay between RNA structure and protein binding. Many previous reports have described how local RNA structure can impact recruitment of *trans*-acting proteins. For example, the iron-responsive RNA-binding protein IRP and nucleolin both show preferential binding to structured RNA targets (54, 55), whereas the ARE binding activities of AUF1 and Hsp70 are inhibited when single-stranded RNA domains are occluded (43). More recently, however, models are developing where protein binding impacts local RNA structure, similar to that proposed for AUF1 in this work and previously (32). For example, under hypoxic stress hnRNP L binds to a translational regulatory domain within the VEGF mRNA 3′UTR, which dramatically alters RNA folding in this region and ultimately enhances translation (56). For both $p37^{AUF1}$ and $p42^{AUF1}$, the first RNA-binding step was associated with diminution of the distance between the 5′ and 3′ termini of an associated RNA substrate (Fig. 6). It is appealing to speculate that the large apparent RNA site sizes observed for P_2R complexes involving $p37^{AUF1}$ or $p42^{AUF1}$ (~33–34 nt) may be coupled to this local condensation of RNA structure, possibly involving recognition of disparate sequence motifs and steric occlusion of intervening substrate nucleotides. One logical functional consequence of protein-dependent changes in local RNA structure is the potential to control accessibility for ancillary RNA-binding factors, a theme that is also gaining recognition. For example, AUF1 and HuR coordinately enhance association of each other with $p16^{INK4}$ mRNA and also assist in recruiting RISC complexes to this transcript (57). Interplay between AUF1 and HuR binding may be a common theme among ARE-containing mRNAs, as gene array studies have identified many transcripts that can bind both proteins simultaneously (50). Protein-dependent changes in local RNA structure may also impact microRNA accessibility, given the contributions of base pair complementarity to the specificity of miRISC·mRNA complex formation. For example, HuR can

enhance recruitment of the microRNA let-7 to c-*myc* mRNA (58), but it can also serve as a negative regulator of microRNA function by blocking miR-122-directed repression of CAT-1 mRNA translation (59). Another RNA-binding protein, Drd1, binds within the 3′UTR of p27 mRNA but blocks miR-221 binding to proximal sites (60).

Based on the distinctive biochemical properties displayed by the different AUF1 isoforms in this work, we anticipate that modulating the expression or activity of individual AUF1 isoforms will enhance the selectivity of post-transcriptional gene regulation. In this manner, the induction of $p45^{AUF1}$ by prostaglandin A_2 in lung carcinoma cells (30) could elicit different physiological consequences than those expected from any other AUF1 isoform, based on the unique $p45^{AUF1}$ concentration dependence on RNP composition and local RNA conformation. However, the complexity of post-transcriptional regulatory control by AUF1 isoforms may be further expanded by the potential for AUF1 proteins to form heterodimers (46) and by post-translational modifications of specific isoforms. For example, $p40^{AUF1}$ phosphorylated within the exon 2-encoded domain at Ser-83 and Ser-87 retains ARE substrates in elongated conformations independent of RNP stoichiometry (31), unlike any unmodified AUF1 isoform studied here (Fig. 6). Because $p37^{AUF1}$ lacks these residues, activation of signaling pathways directing $p40^{AUF1}$ phosphorylation at these sites could thus selectively regulate the function of $p40^{AUF1}$, without altering the other major cytoplasmic isoform. Cellular radiolabeling, phosphoamino acid-specific antibodies, and two-dimensional Western analyses further indicate that other AUF1 isoforms can also be post-translationally modified on Ser, Thr, and Tyr residues (21, 28, 61–63), hinting at a geometrically expanding array of regulatory possibilities.

Finally, the isoform-specific models of AUF1 RNP assembly described in this study may help explain some conflicting literature reports of AUF1 function, particularly in cases where individual AUF1 isoforms are overexpressed in cells. Suppression of AUF1 using siRNA-based approaches is most frequently associated with stabilization of mRNA substrates, consistent with a general mRNA-destabilizing role for at least some AUF1 proteins (17, 64, 65). However, ectopic overexpression of AUF1 proteins has prompted much more variable conclusions, associated with both mRNA-destabilizing (18) and -stabilizing (66) roles. This dichotomy was most clearly presented in a recent work showing that both siRNA-directed suppression and ectopic overexpression of AUF1 stabilized a reporter mRNA containing the ARE from IL-6 mRNA (16). Although some of these apparent contradictions may reflect differences in mRNA targets or cell types, we suggest that the mRNA metabolic consequences of modulating AUF1 levels may be strongly influenced by isoform-dependent effects on the sensitivity of RNP size and conformation to changes in protein concentrations. For example, the weak K_2 values resolved for $p37^{AUF1}$ and $p40^{AUF1}$ binding to ARE substrates (Table 3) indicates that RNPs assembled from these isoforms would exist principally as P_2R complexes across a wide range of protein concentrations (modeled in Fig. 6*A* for $p37^{AUF1}$). It is therefore possible that the P_2R complex represents the major cellular $p37^{AUF1}$ or $p40^{AUF1}$ RNP under normal physiological conditions. However, dramatic overexpression of these isoforms would be expected to shift the distribution of their cognate RNPs in favor of P_4R complexes, which may direct very different functional consequences on targeted RNA substrates.

Acknowledgment—We thank Li-Yen R. Hu for valuable technical discussions.

REFERENCES

1. Guhaniyogi, J., and Brewer, G. (2001) *Gene* **265,** 11–23
2. Garneau, N. L., Wilusz, J., and Wilusz, C. J. (2007) *Nat. Rev. Mol. Cell Biol.* **8,** 113–126
3. Chen, C. Y., and Shyu, A. B. (1995) *Trends Biochem. Sci.* **20,** 465–470
4. Bakheet, T., Williams, B. R., and Khabar, K. S. (2006) *Nucleic Acids Res.* **34,** D111–D114
5. Wilson, G. M., and Brewer, G. (1999) *Prog. Nucleic Acid Res. Mol. Biol.* **62,** 257–291
6. Barreau, C., Paillard, L., and Osborne, H. B. (2005) *Nucleic Acids Res.* **33,** 7138–7150
7. Jing, Q., Huang, S., Guth, S., Zarubin, T., Motoyama, A., Chen, J., Di Padova, F., Lin, S. C., Gram, H., and Han, J. (2005) *Cell* **120,** 623–634
8. Calin, G. A., Cimmino, A., Fabbri, M., Ferracin, M., Wojcik, S. E., Shimizu, M., Taccioli, C., Zanesi, N., Garzon, R., Aqeilan, R. I., Alder, H., Volinia, S., Rassenti, L., Liu, X., Liu, C. G., Kipps, T. J., Negrini, M., and Croce, C. M. (2008) *Proc. Natl. Acad. Sci. U.S.A.* **105,** 5166–5171
9. Fan, X. C., and Steitz, J. A. (1998) *EMBO J.* **17,** 3448–3460
10. Peng, S. S., Chen, C. Y., Xu, N., and Shyu, A. B. (1998) *EMBO J.* **17,** 3461–3470
11. Lai, W. S., Carballo, E., Strum, J. R., Kennington, E. A., Phillips, R. S., and Blackshear, P. J. (1999) *Mol. Cell. Biol.* **19,** 4311–4323
12. Lai, W. S., Carballo, E., Thorn, J. M., Kennington, E. A., and Blackshear, P. J. (2000) *J. Biol. Chem.* **275,** 17827–17837
13. Gherzi, R., Lee, K. Y., Briata, P., Wegmüller, D., Moroni, C., Karin, M., and Chen, C. Y. (2004) *Mol. Cell* **14,** 571–583
14. Chen, C. Y., Gherzi, R., Ong, S. E., Chan, E. L., Raijmakers, R., Pruijn, G. J., Stoecklin, G., Moroni, C., Mann, M., and Karin, M. (2001) *Cell* **107,** 451–464
15. Brewer, G., Saccani, S., Sarkar, S., Lewis, A., and Pestka, S. (2003) *J. Interferon Cytokine Res.* **23,** 553–564
16. Paschoud, S., Dogar, A. M., Kuntz, C., Grisoni-Neupert, B., Richman, L., and Kühn, L. C. (2006) *Mol. Cell. Biol.* **26,** 8228–8241
17. Raineri, I., Wegmueller, D., Gross, B., Certa, U., and Moroni, C. (2004) *Nucleic Acids Res.* **32,** 1279–1288
18. Sarkar, B., Xi, Q., He, C., and Schneider, R. J. (2003) *Mol. Cell. Biol.* **23,** 6685–6693
19. Zhang, T., Kruys, V., Huez, G., and Gueydan, C. (2002) *Biochem. Soc. Trans.* **30,** 952–958
20. Wagner, B. J., DeMaria, C. T., Sun, Y., Wilson, G. M., and Brewer, G. (1998) *Genomics* **48,** 195–202
21. Zhang, W., Wagner, B. J., Ehrenman, K., Schaefer, A. W., DeMaria, C. T., Crater, D., DeHaven, K., Long, L., and Brewer, G. (1993) *Mol. Cell. Biol.* **13,** 7652–7665
22. DeMaria, C. T., Sun, Y., Long, L., Wagner, B. J., and Brewer, G. (1997) *J. Biol. Chem.* **272,** 27635–27643
23. Brewer, G. (1991) *Mol. Cell. Biol.* **11,** 2460–2466
24. Lu, J. Y., Bergman, N., Sadri, N., and Schneider, R. J. (2006) *RNA* **12,** 883–893
25. Liao, B., Hu, Y., and Brewer, G. (2007) *Nat. Struct. Mol. Biol.* **14,** 511–518
26. Arao, Y., Kuriyama, R., Kayama, F., and Kato, S. (2000) *Arch. Biochem. Biophys.* **380,** 228–236
27. Mili, S., Shu, H. J., Zhao, Y., and Piñol-Roma, S. (2001) *Mol. Cell. Biol.* **21,** 7307–7319

28. Wilson, G. M., Lu, J., Sutphen, K., Sun, Y., Huynh, Y., and Brewer, G. (2003) *J. Biol. Chem.* **278,** 33029–33038
29. Ing, N. H., Massuto, D. A., and Jaeger, L. A. (2008) *J. Biol. Chem.* **283,** 1764–1772
30. Lin, S., Wang, W., Wilson, G. M., Yang, X., Brewer, G., Holbrook, N. J., and Gorospe, M. (2000) *Mol. Cell. Biol.* **20,** 7903–7913
31. Wilson, G. M., Lu, J., Sutphen, K., Suarez, Y., Sinha, S., Brewer, B., Villanueva-Feliciano, E. C., Ysla, R. M., Charles, S., and Brewer, G. (2003) *J. Biol. Chem.* **278,** 33039–33048
32. Wilson, G. M., Sutphen, K., Moutafis, M., Sinha, S., and Brewer, G. (2001) *J. Biol. Chem.* **276,** 38400–38409
33. Heyduk, T., Ma, Y., Tang, H., and Ebright, R. H. (1996) *Methods Enzymol.* **274,** 492–503
34. Chen, C. Y., Chen, T. M., and Shyu, A. B. (1994) *Mol. Cell. Biol.* **14,** 416–426
35. Wilson, G. M., Sun, Y., Lu, H., and Brewer, G. (1999) *J. Biol. Chem.* **274,** 33374–33381
36. Wilson, G. M., Sutphen, K., Chuang, Ky., and Brewer, G. (2001) *J. Biol. Chem.* **276,** 8695–8704
37. Jancarik, J., Pufan, R., Hong, C., Kim, S. H., and Kim, R. (2004) *Acta Crystallogr. D Biol. Crystallogr.* **60,** 1670–1673
38. Wilson, G. M., and Brewer, G. (1999) *Methods* **17,** 74–83
39. Weber, G. (1952) *Biochem. J.* **51,** 145–155
40. Wilson, G. M. (2005) in *Reviews in Fluorescence* (Geddes, C. D., and Lakowicz, J. R., eds) Vol. 2, pp. 223–243, Springer Science+Business Media, New York
41. Lohman, T. M., and Bujalowski, W. (1991) *Methods Enzymol.* **208,** 258–290
42. Bujalowski, W., and Jezewska, M. J. (2000) in *Spectrophotometry and Spectrofluorimetry* (Gore, M. G., ed) pp. 141–165, Oxford University Press, Oxford, UK
43. Fialcowitz, E. J., Brewer, B. Y., Keenan, B. P., and Wilson, G. M. (2005) *J. Biol. Chem.* **280,** 22406–22417
44. Lakowicz, J. R. (1999) *Principles of Fluorescence Spectroscopy*, 2nd Ed., pp. 367–394, Kluwer Academic/Plenum, New York
45. Norman, D. G., Grainger, R. J., Uhrín, D., and Lilley, D. M. (2000) *Biochemistry* **39,** 6317–6324
46. Sarkar, B., Lu, J. Y., and Schneider, R. J. (2003) *J. Biol. Chem.* **278,** 20700–20707
47. Bujalowski, W., and Jezewska, M. J. (1995) *Biochemistry* **34,** 8513–8519
48. Mazan-Mamczarz, K., Kuwano, Y., Zhan, M., White, E. J., Martindale, J. L., Lal, A., and Gorospe, M. (2009) *Nucleic Acids Res.* **37,** 204–214
49. Glaser, N. D., Lukyanenko, Y. O., Wang, Y., Wilson, G. M., and Rogers, T. B. (2006) *Am. J. Physiol. Heart Circ. Physiol.* **291,** H1183–H1192
50. Lal, A., Mazan-Mamczarz, K., Kawai, T., Yang, X., Martindale, J. L., and Gorospe, M. (2004) *EMBO J.* **23,** 3092–3102
51. Eversole, A., and Maizels, N. (2000) *Mol. Cell. Biol.* **20,** 5425–5432
52. Jezewska, M. J., Rajendran, S., and Bujalowski, W. (1998) *J. Mol. Biol.* **284,** 1113–1131
53. Okunola, H. L., and Krainer, A. R. (2009) *Mol. Cell. Biol.* **29,** 5620–5631
54. Addess, K. J., Basilion, J. P., Klausner, R. D., Rouault, T. A., and Pardi, A. (1997) *J. Mol. Biol.* **274,** 72–83
55. Bouvet, P., Allain, F. H., Finger, L. D., Dieckmann, T., and Feigon, J. (2001) *J. Mol. Biol.* **309,** 763–775
56. Ray, P. S., Jia, J., Yao, P., Majumder, M., Hatzoglou, M., and Fox, P. L. (2009) *Nature* **457,** 915–919
57. Chang, N., Yi, J., Guo, G., Liu, X., Shang, Y., Tong, T., Cui, Q., Zhan, M., Gorospe, M., and Wang, W. (2010) *Mol. Cell. Biol.* **30,** 3875–3886
58. Kim, H. H., Kuwano, Y., Srikantan, S., Lee, E. K., Martindale, J. L., and Gorospe, M. (2009) *Genes Dev.* **23,** 1743–1748
59. Bhattacharyya, S. N., Habermacher, R., Martine, U., Closs, E. I., and Filipowicz, W. (2006) *Cold Spring Harbor Symp. Quant. Biol.* **71,** 513–521
60. Kedde, M., Strasser, M. J., Boldajipour, B., Oude Vrielink, J. A., Slanchev, K., le Sage, C., Nagel, R., Voorhoeve, P. M., van Duijse, J., Ørom, U. A., Lund, A. H., Perrakis, A., Raz, E., and Agami, R. (2007) *Cell* **131,** 1273–1286
61. Fawal, M., Armstrong, F., Ollier, S., Dupont, H., Touriol, C., Monsarrat, B., Delsol, G., Payrastre, B., and Morello, D. (2006) *Blood* **108,** 2780–2788
62. Blum, J. L., Samarel, A. M., and Mestril, R. (2005) *Am. J. Physiol. Heart Circ. Physiol.* **289,** H2543–H2550
63. Levi, R., Ben-Dov, I. Z., Lavi-Moshayoff, V., Dinur, M., Martin, D., Naveh-Many, T., and Silver, J. (2006) *J. Am. Soc. Nephrol.* **17,** 107–112
64. Mawji, I. A., Robb, G. B., Tai, S. C., and Marsden, P. A. (2004) *J. Biol. Chem.* **279,** 8655–8667
65. Pautz, A., Linker, K., Altenhöfer, S., Heil, S., Schmidt, N., Art, J., Knauer, S., Stauber, R., Sadri, N., Pont, A., Schneider, R. J., and Kleinert, H. (2009) *J. Biol. Chem.* **284,** 2755–2766
66. Xu, N., Chen, C. Y., and Shyu, A. B. (2001) *Mol. Cell. Biol.* **21,** 6960–6971